

Search for Excited Electrons in the $ee\gamma$ Channel

The DØ Collaboration
URL <http://www-d0.fnal.gov>
(Dated: March 7, 2007)

We present results of the first search for excited electron production at the D0 experiment. The excited electron e^* is assumed to be produced via contact interactions: $p\bar{p} \rightarrow ee^*$. For the subsequent decay we consider the electromagnetic decay mode $e^* \rightarrow e\gamma$, resulting in the final state $ee\gamma$. The analysis is based on data taken at $\sqrt{s} = 1.96$ TeV in Tevatron Run II, corresponding to an integrated luminosity of 1.0 fb^{-1} .

No excess is observed in the data with respect to the Standard Model expectation, and upper limits on the excited electron production cross section times branching fraction are derived. These limits correspond to a lower limit of $m_{e^*} > 756$ GeV at 95% CL for a compositeness scale $\Lambda = 1$ TeV. We also interpret the result in terms of limits on Λ as a function of m_{e^*} .

I. INTRODUCTION

Several models attempt to explain the observation of three families of fundamental fermions, by postulating that quarks and leptons are composed of scalar and spin-1/2 particles. Due to this underlying substructure, compositeness models [1] imply a large spectrum of excited states [1, 2]. Exchange of these substructure particles leads to ‘contact-interactions’ (CI) between quarks and leptons [2].

In the analysis presented here, production of single excited electrons via CI, and their subsequent electroweak decay into electron and photon are considered. The gauge particle mediated (GM) production cross section of excited electrons is neglected since it is expected to be smaller than 1% of the CI cross section [3]. However, the predictions of such models could be confronted with the results presented here, because acceptance and efficiencies are expected to be similar to the CI model.

The relevant parameters for excited electron production are the excited electron mass m_{e^*} as well as the compositeness scale parameter Λ . The contact interaction can be described by an effective four-fermion Lagrangian of the form

$$\mathcal{L}_{CI} = \frac{g^2}{2\Lambda^2} j^\mu j_\mu, \quad (1)$$

where j_μ is the fermion current

$$j_\mu = \eta_L \bar{f}_L \gamma_\mu f_L + \eta'_L \bar{f}^*_L \gamma_\mu f^*_L + \eta''_L \bar{f}^*_L \gamma_\mu f_L + h.c. + (L \rightarrow R). \quad (2)$$

The Standard Model (SM) and excited fermions are denoted by f and f^* , respectively; g^2 is chosen to be 4π , the η factors for the left-handed currents are conventionally set to one, and the right-handed currents are set to zero.

For the partial width of the gauge-mediated decay, the parameters f and f' are also relevant. They are determined by the composite dynamics and control the coupling between photons, excited electrons and excited neutrinos. All branching fractions are calculated for the GM decay parameters $f = f' = 1$ [2]. The total width is $\Gamma > 1$ GeV for $100 \leq m_{e^*} \leq 1000$ GeV, thus lifetime effects can be neglected in this analysis.

The contribution of the CI decays to the total width is taken into account as a corresponding reduction of the branching fraction of the channel $e^* \rightarrow e \gamma$, using the branching fraction (BF) as given by [2].

Limits on heavy excited electrons have previously been set at LEP [4], HERA [5], and by the CDF experiment [6]. Only the CDF limit is directly comparable to the present analysis because the LEP and HERA results assume production via GM and depend on the relevant couplings. Due to the center-of-mass energy available, the LEP sensitivity for single production of excited leptons is limited to $m_{e^*} \lesssim 200$ GeV, and correspondingly $m_{e^*} \lesssim 250$ GeV for HERA.

II. DATA SAMPLES AND MONTE CARLO SIMULATION

The analysis is based on data collected with the D0 detector [7] between August 2002 and February 2006, corresponding to an integrated luminosity of $\mathcal{L} = 1013 \pm 62$ pb $^{-1}$ [8]. The D0 detector includes a central tracking system, comprised of a silicon microstrip tracker (SMT) and a central fiber tracker (CFT), both located within a 2 T superconducting solenoidal magnet. The SMT has $\approx 800,000$ individual strips, with typical pitch of 50 – 80 μm , and a design optimized for tracking and vertexing capability at pseudorapidities¹ of $|\eta| < 2.5$. The CFT has eight coaxial barrels, each supporting two doublets of scintillating fibers of 0.835 mm diameter, one doublet being parallel to the collision axis, and the other alternating by $\pm 3^\circ$ relative to the axis. Three liquid argon and uranium calorimeters provide coverage out to $|\eta| \approx 4.2$: a central section (CC) covering $|\eta|$ up to ≈ 1.1 , and two end calorimeters (EC). A muon system resides beyond the calorimetry, and consists of a layer of tracking detectors and scintillation trigger counters before 1.8 T iron toroids, followed by two similar layers after the toroids. Luminosity is measured using scintillator arrays located in front of the end calorimeter cryostats, covering $2.7 < |\eta| < 4.4$.

Trigger and data acquisition systems are designed to accommodate the high luminosities of the Tevatron Run II. Based on information from tracking, calorimetry, and muon systems, the output of the first two levels of the trigger is used to limit the rate for accepted events to < 1 kHz, relying on hardware and firmware. The third and final level of the trigger uses software algorithms and a computing farm to reduce the output rate to a maximum of ≈ 100 Hz,

¹ The pseudorapidity η is defined as $\eta = -\ln(\tan(\theta/2))$. We use the polar angle θ relative to the proton beam direction, and ϕ is the azimuthal angle, all measured with respect to the geometric center of the detector.

which is written to tape. For the present analysis, events are required to pass at least one single or dielectron trigger, yielding close to 100% efficiency.

The main SM contribution to the $ee\gamma$ final state is expected to be the Drell-Yan (DY) process $Z/\gamma^* \rightarrow ee$ where an additional photon is radiated. Smaller contributions are expected from: $Z/\gamma^* \rightarrow \tau\tau$, the diboson channels WW , WZ , and ZZ , as well as from $W \rightarrow e\nu$ and $t\bar{t}$ production. The SM background Monte Carlo (MC) samples were generated with the PYTHIA [9] Monte Carlo program version 6.3. The DY expectation (as well as $W \rightarrow e\nu$) has been corrected using the next-to-next-to-leading order (NNLO) calculation from [10]. In addition, the transverse momentum (p_T) distribution of the e^+e^- pair was corrected to match the distribution observed in the data. For diboson production, the next-to-leading order cross sections from [11] are used. The $t\bar{t}$ production cross section has been taken from [12]. The CTEQ6L1 parton distribution functions (PDF) [13] are used for the generation of all MC samples.

Additional background is possible from events with two or more jets and a photon, where the jets are misidentified as electrons. The contribution of this ‘‘QCD background’’ was estimated from the data, as described later.

The signal process ($p\bar{p} \rightarrow ee^* \rightarrow ee\gamma$) was generated with PYTHIA version 6.3. The BF for the decay $e^* \rightarrow e\gamma$ normalized to all gauge particle decay modes ($e^* \rightarrow \nu W$, $e^* \rightarrow e\gamma$, and $e^* \rightarrow eZ$) is 30% for masses above 300 GeV, and for smaller e^* masses it increases up to 73% at $m_{e^*} = 100$ GeV. The contribution from decays via contact interactions, which are not implemented in PYTHIA, varies between a few percent of all decays for $\Lambda \gg m_{e^*}$ and 92% for $\Lambda = m_{e^*}$ [2]. This has been taken into account for the signal expectation (see Table I). The leading-order cross section calculated with PYTHIA has been corrected to NNLO [10]; the corresponding correction factor varies between 1.3 and 1.5, depending on the invariant mass of the ee^* system, and assuming that the calculation for DY production is applicable.

Monte Carlo events, both for SM and signal, have been passed through a detector simulation based on the GEANT [14] package, and reconstructed using the same reconstruction program as the data.

Efficiencies for electron and photon identification and track reconstruction have been determined from the simulation. To verify the simulation and to estimate systematic uncertainties, the efficiencies have also been calculated from data samples, using $Z \rightarrow e^+e^-$ candidate events. Differences between the efficiency determinations from data and simulation are corrected in the simulation.

m_{e^*} [GeV]	$\sigma_{prod}^{CI}(LO)$ [pb]	BF	$\sigma_{prod}^{CI}(NNLO) \times \text{BF}$ [pb]
100	91.8	0.27	34.8
200	24.6	0.21	7.29
300	10.4	0.15	2.22
400	4.37	0.11	0.67
500	2.01	0.08	0.23
600	0.92	0.06	0.078
700	0.31	0.05	0.021
800	0.12	0.04	0.0061
900	0.035	0.03	0.0015
1000	0.010	0.03	0.00037

TABLE I: Generated MC samples for the e^* production. Given are the leading-order cross sections, the BF for $e^* \rightarrow e\gamma$ relative to all possible decays through GM and CI, and the NNLO cross section times BF. All numbers are for a compositeness scale $\Lambda = 1$ TeV. Between 3500 and 5000 events have been generated for each value of m_{e^*} .

III. EVENT SELECTION

At least two isolated high p_T electrons are required; they must both fulfill the following requirements:

- Transverse momentum $p_T > 25$ GeV for the leading electron, and $p_T > 15$ GeV for the second leading electron. The p_T is reconstructed from calorimeter clusters.
- Electromagnetic (EM) fraction of energy deposited in the EM part of the calorimeter: $emfrac > 0.9$.
- Isolation of the electron candidates in the calorimeter: $iso = (E_{tot}(0.4) - E_{em}(0.2))/E_{em}(0.2) < 0.2$, where $E_{tot}(0.4)$ and $E_{em}(0.2)$ denote the energy deposited in the calorimeter and only its electromagnetic section in cones of size $\Delta R = \sqrt{(\Delta\eta)^2 + (\Delta\phi)^2} = 0.4$ and 0.2, respectively.

- Within geometric coverage of the calorimeters and tracking systems: $|\eta_{det}| < 1.1$ (CC) or $1.5 < |\eta_{det}| < 2.5$ (EC), where η_{det} is measured with respect to the center of the detector.
- Longitudinal and transverse shower shape should be consistent with that expected from an electron.
- Calorimeter cluster should have a central track pointing to it.
- Separation between electrons: $\Delta R > 0.4$.
- Events where the two electrons are reconstructed in opposite EC's are rejected.

Due to the different systematic effects in the CC and EC calorimeters, the events were divided into the three topologies CC/CC, CC/EC, and EC/EC, depending on the location of the electrons in the detector. For the CC/CC and CC/EC topologies, the invariant mass of the two selected electrons is shown in Fig. 1.

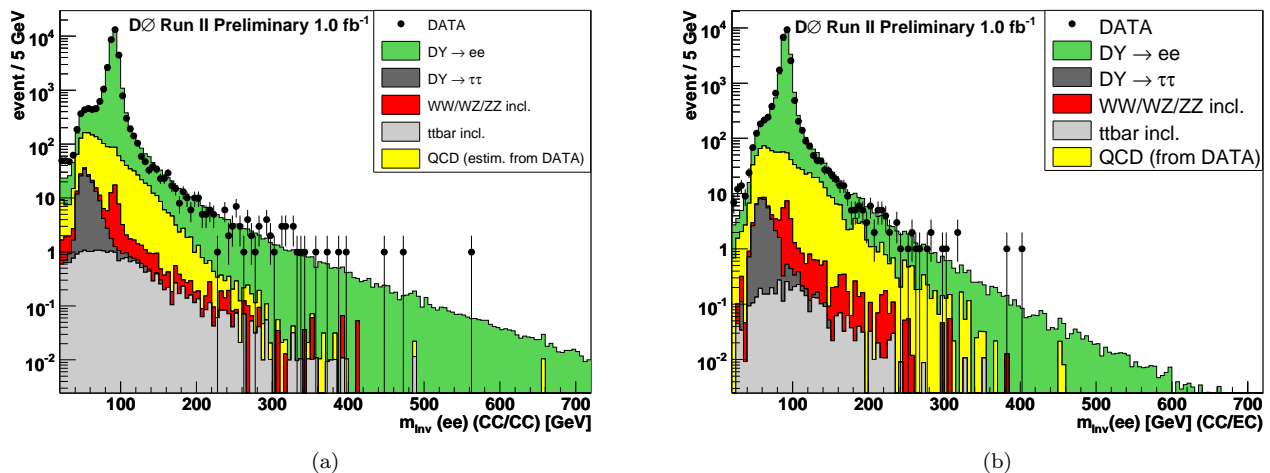


FIG. 1: The invariant mass of the two selected electrons: (a) both electrons are detected in the CC, (b) one electron is detected in CC, another one in EC.

The QCD background estimate was obtained in the following way. Events were selected from the data which fulfill all of the criteria listed above, with the exception of inverting the shower shape requirements. The resulting data sample is dominated by “fake” electrons, and has a negligible signal contribution. In addition, the track match requirement was relaxed in that only one of the two EM objects was required to be track matched. Due to a possible bias from p_T -dependent shower shape requirements in the trigger, the p_T distribution of the leading and second leading EM object was corrected to match the distribution observed in the QCD contribution to the dielectron sample. In a last step, the QCD sample was normalized such that the sum of QCD background and other SM backgrounds agree with the data in the mass interval $30 < m(ee) < 65$ GeV, where the expected signal contribution is negligible.

The sum of all backgrounds provides a reasonable description of the data, as can be seen in Fig. 1. We find 62930 events in the data, with a SM expectation of $61560 \pm 120(\text{stat.}) \pm 6553(\text{syst.})$ events.

The $ee\gamma$ Selection

The $ee\gamma$ sample is obtained by requiring an additional photon with the following requirements:

- A high- p_T electromagnetic cluster with $p_T > 15$ GeV within $|\eta_{det}| < 1.1$ or $1.5 < |\eta_{det}| < 2.5$.
- No associated track in the central tracking system.
- Isolation from other tracks: the sum of the transverse momenta of tracks within a hollow cone defined by $0.05 < \Delta R < 0.4$ around the photon direction has to be below 2 GeV.
- Tight criteria to reduce the rate of jets misidentified as photons: $emfrac > 0.97$, $iso < 0.07$, additional requirements on the shower shape in the third layer of the EM calorimeter, and fiducial cuts to ensure a good description by the simulation.

- Separation $\Delta R > 0.4$ to both electrons.

With these requirements, 259 events remain in the data, while $232 \pm 3(\text{stat.}) \pm 29(\text{syst.})$ events are expected from SM processes. The invariant mass of the final $ee\gamma$ sample is displayed in Fig. 2. The data are described reasonably well by the sum of the SM processes. For the $DY \rightarrow ee$ background, we show separately the contributions from events with a ‘true’ photon, and the events where a jet was misidentified as a photon. The total SM expectation is dominated by DY events with a true photon, which contribute about 225 events.

Additional control distributions for the two electrons and the photon are shown in Fig. 3. The transverse momentum and the η distributions of the three selected objects as well as the distribution of the separation ΔR between the electrons and the photon show a good agreement of data and SM backgrounds.

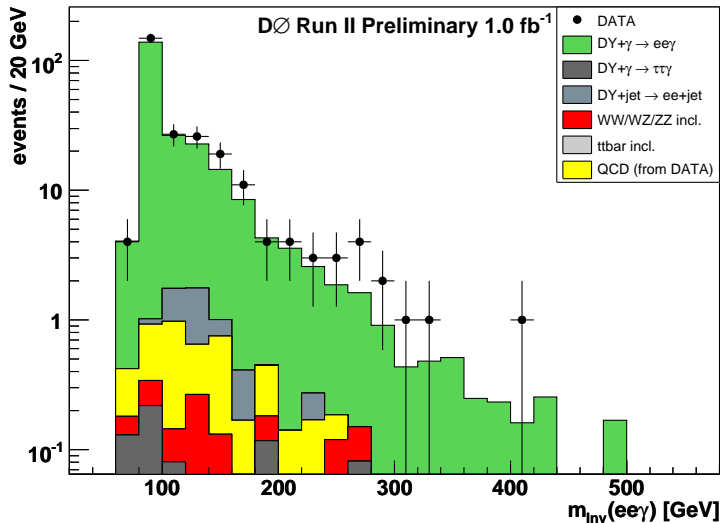


FIG. 2: The invariant mass $m(ee\gamma)$ of the two selected electrons and the photon.

Optimization

The excited electron decay $e^* \rightarrow e\gamma$ would be observable as a resonance in the $e\gamma$ invariant mass. Therefore a cut on the invariant mass of the photon and one of the electrons should lead to a better separation of the possible signal from the SM background. In addition, for a light excited electron, the decay electron and the photon are expected to be separated by small angles, so placing a requirement on the separation ΔR between the lower p_T electron and the photon may allow to increase the sensitivity of the analysis. In the following we describe the optimization steps we have performed.

The invariant mass of the hypothetical excited electron can be reconstructed by selecting the photon and one of the electrons (see Fig. 4). The possible signal is clearly separated from the SM backgrounds. From a study of the signal simulation we find that for masses $m_{e^*} \leq 200$ GeV, the lower p_T electron is with high probability the electron from the e^* decay, and therefore this combination leads to the better signal to background ratio. For heavier e^* masses, where backgrounds are small, we use a different algorithm to determine the decay electron: the combination with an invariant mass closest to the searched e^* mass is chosen.

For further selection criteria, we use the average expected cross section limit for each value of m_{e^*} to determine optimal methods and cut values:

- Two options are evaluated for the optimal choice of a cut on the invariant $e\gamma$ mass: a symmetrical mass window around the excited electron mass under study, and a lower mass cut. For both options, possible selection values are tested, and the optimal one is chosen. In all cases, a lower mass cut yields the best expected limits.
- We also compared the expected limits with and without including events with both electrons detected in the calorimeter end caps. The influence of including events with the photon reconstructed in one of the end caps, where the backgrounds from wrongly identified photons are higher, was analyzed as well. As a result, only for

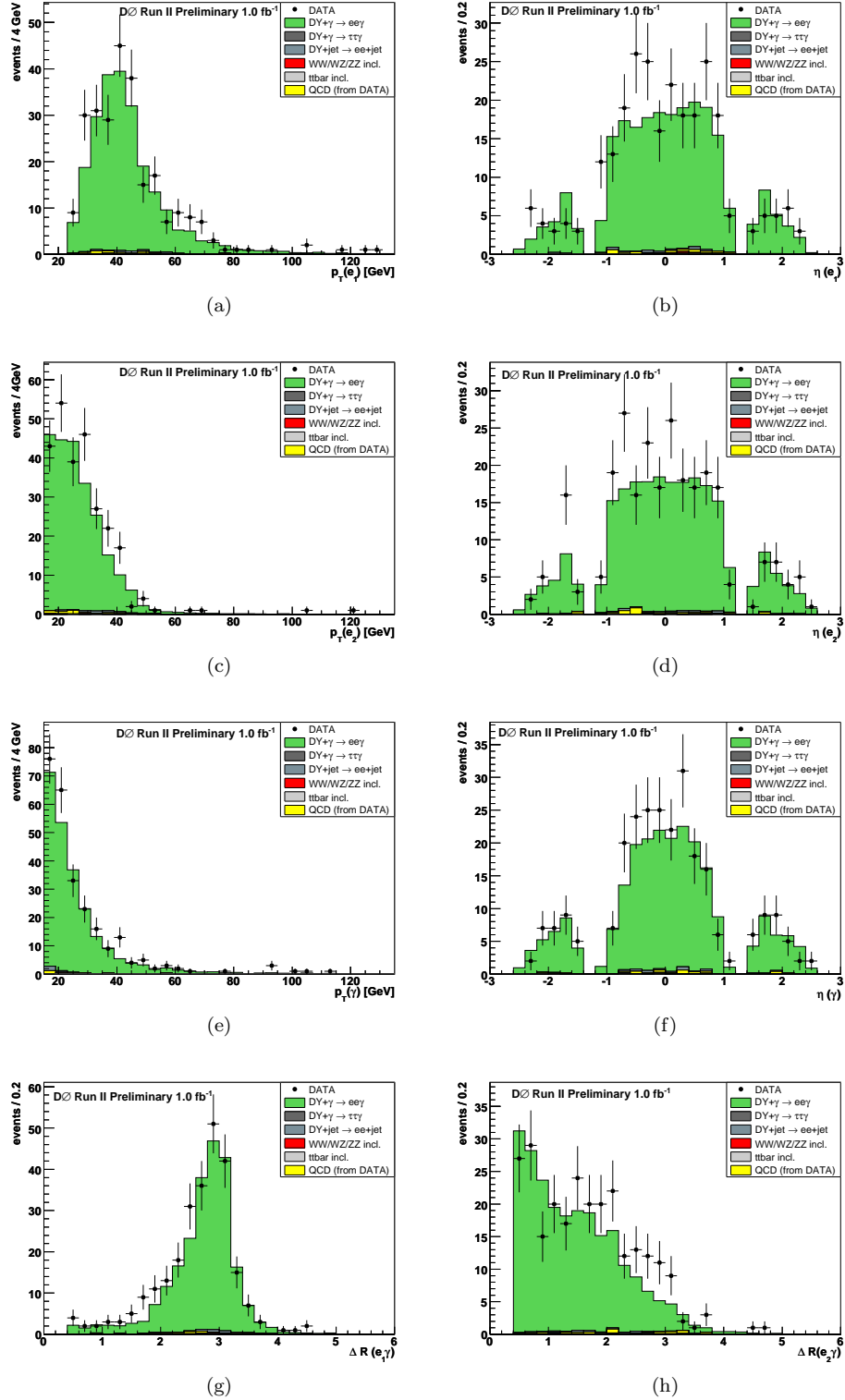


FIG. 3: Control distributions for the $ee\gamma$ sample: (a,c,e) the p_T distributions of the three EM objects, (b,d,f) the η distributions, and (g,h) the separation ΔR between the electrons and the photon.

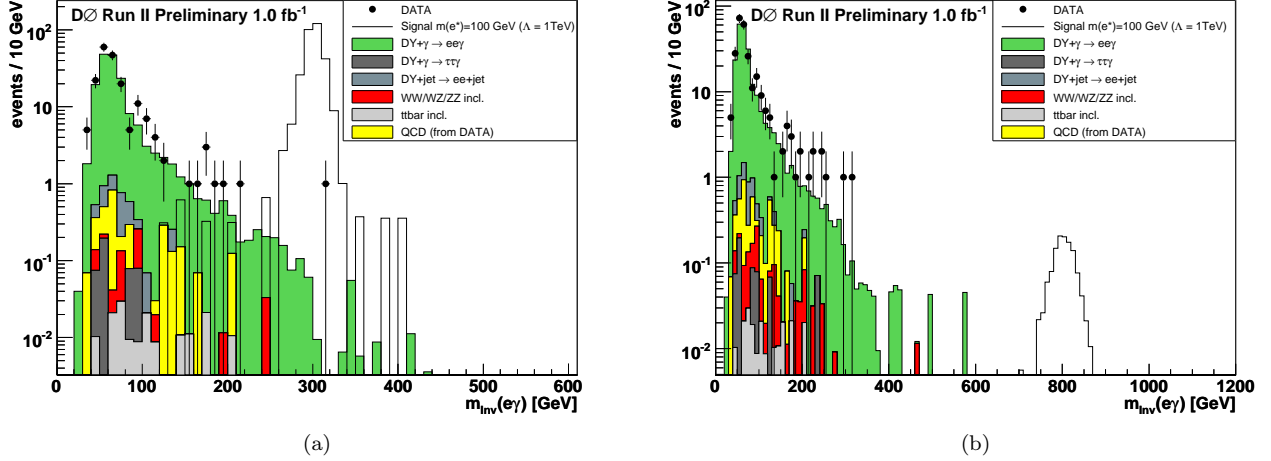


FIG. 4: The invariant mass of the excited electron decay particles e and γ for masses of (a) $m_{e^*} = 300$ GeV and (b) 800 GeV. These distributions were obtained by selecting the $e\gamma$ combination closest to the searched mass. In (a), events with electrons in the EC/EC topology as well as events where the photon is reconstructed in one of the EC's are not included.

$m_{e^*} > 300$ GeV all EC electron and photon combinations were kept, in order to maximize the acceptance and keep the search as general as possible.

- For small excited electron masses the separation ΔR between the electron with lower transverse momentum and the photon is a good quantity to separate signal from background (see Fig. 5). Again, the cut values were optimized by comparing expected limits.

The final selection criteria are summarized in Table II.

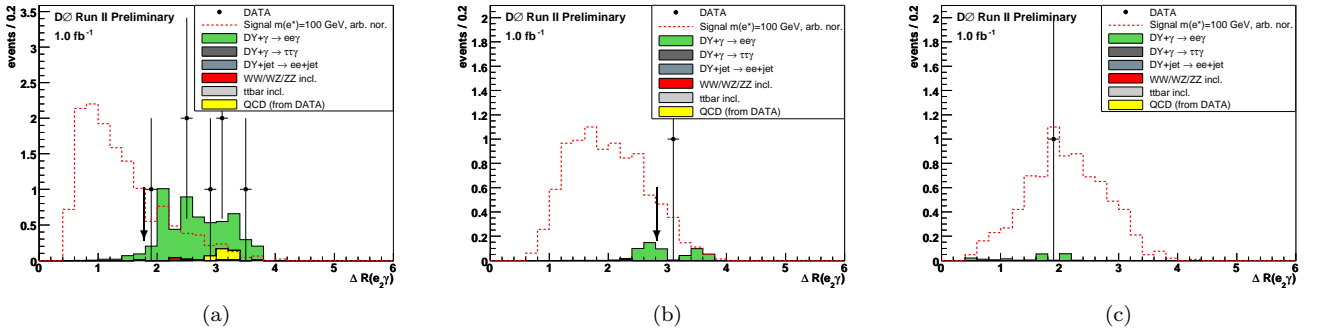


FIG. 5: The separation ΔR of the lower p_T electron and the photon after all other cuts for (a) $m_{e^*} = 100$ GeV, (b) 200 GeV, and (c) 300 GeV. The selection criteria for $m_{e^*} = 100$ GeV and 200 GeV are indicated by arrows.

Systematic Uncertainties

The reconstruction and identification efficiency for high p_T isolated electrons is known to a precision of 2.5% per electron. For photons, the uncertainty depends on the transverse momentum and varies between 3.5% for $p_T = 20$ GeV and 2.0% for $p_T > 30$ GeV.

The uncertainties on the trigger efficiency are estimated as $^{+0\%}_{-3\%}$.

The normalization uncertainty due to the measurement of the integrated luminosity is 6.1% [8].

For the misidentification rate of photons by jets in the Drell-Yan sample a systematic uncertainty of 100% is taken, which is still negligible due to the small estimated rate of this background.

m_{e^*} [GeV]	$m(e_2, \gamma)$ [GeV]	$m(e\gamma)$ [GeV] (closest to m_{e^*})	EC/EC	EC γ	$\Delta R(e_2, \gamma)$
100	> 90	–	no	no	< 1.8
200	> 165	–	no	no	< 2.8
300	–	> 290	no	no	all
400	–	> 370	yes	yes	all
500	–	> 445	yes	yes	all
600	–	> 515	yes	yes	all
700	–	> 600	yes	yes	all
800	–	> 705	yes	yes	all
900	–	> 800	yes	yes	all
1000	–	> 900	yes	yes	all

TABLE II: The selection cuts optimized with respect to the best expected limit. The second and the third columns show the lower mass cuts. The next column shows if events with both electrons in the EC were rejected, the fifth if events with photons detected in the EC are rejected, and the very right one the upper value for the separation between the second leading electron and the photon. Events where both electrons were detected in opposite EC's are always rejected.

The uncertainty in the QCD background determination is estimated by varying the selection criteria by which it is obtained. An uncertainty of 25% on the corresponding background is determined.

The uncertainty on the SM cross sections of typically 4% is dominated by the DY process and the uncertainty from the choice of PDF and renormalization and factorization scales. The same uncertainties are assumed for the signal process. In addition, the effect of the PDF uncertainty on the acceptance is evaluated using the CTEQ 6.1M error set [13], and found to vary between 2% ($m_{e^*} = 100$ GeV) and 7% ($m_{e^*} = 1$ TeV).

The total uncertainty on the signal cross section due to PDF uncertainties and unknown higher order corrections is estimated to 10% and is taken into account in the calculation of mass limits (see Sec. IV).

IV. RESULTS

The selected data and the expected SM background, as well as the signal efficiency after all cuts are listed in Table III. Statistical and systematic uncertainties are given as well. Data and SM expectation agree, and no significant excess is observed for any e^* candidate mass, so upper limits can be set on the contact interaction production cross section of excited electrons and the subsequent decay into electron and photon. Lower limits on the mass of the excited electron m_{e^*} are set, as well as for the compositeness scale Λ as a function of m_{e^*} . The limits are calculated using the Bayesian approach and Poisson statistics [15].

The results of the limit calculation with 95% confidence level are listed in Table III, as well as the average expected limits, and shown in Fig. 6. Also shown in Fig. 6 are the theoretical cross sections for several values of the compositeness scale ($\Lambda = m_{e^*}, 1$ TeV, 2 TeV, 3 TeV, 4 TeV, 5 TeV), including their uncertainties. The lower mass limit for excited electrons was determined to

$$m_{e^*} > 756 \text{ GeV} \quad \text{at } 95\% \text{ CL},$$

assuming $\Lambda = 1$ TeV. For $\Lambda = m_{e^*}$ the resulting lower mass bound is 796 GeV.

We also derived a limit for a scenario where decays through contact interactions are neglected, in order to compare with a result by the CDF Collaboration [6]. In that case, we find $m_{e^*} > 946$ GeV for $\Lambda = m_{e^*}$, while the CDF result was $m_{e^*} > 879$ GeV. Thus the mass bound presented here is the most stringent limit derived so far².

The limits on the cross section can be interpreted directly as limits on the compositeness scale Λ . The area excluded by the present analysis in the plane of Λ and m_{e^*} is displayed in Fig. 7.

² In addition, the CDF mass limit has been derived with a theoretical cross section too large by a factor of two, due to a bug in older versions of PYTHIA; later searches for excited muons both by D0 and CDF, as well as the present analysis, have used the corrected cross section.

m_{e^*} [GeV]	Data	SM Expectation	Signal ϵ [%]	$\sigma_{95}^{obs.} \times BF(e^* \rightarrow e\gamma)[pb]$	$\sigma_{95}^{exp.} \times BF(e^* \rightarrow e\gamma)[pb]$
100	0	$0.31 \pm 0.08 \pm 0.03$	$13.2 \pm 0.6 \pm 1.6$	0.024	0.027
200	0	$0.20 \pm 0.09 \pm 0.02$	$13.8 \pm 0.5 \pm 1.8$	0.021	0.025
300	1	$0.28 \pm 0.10 \pm 0.03$	$22.1 \pm 0.7 \pm 2.6$	0.021	0.016
400	0	$0.22 \pm 0.17 \pm 0.02$	$28.3 \pm 0.8 \pm 3.3$	0.011	0.012
500	0	$0.018 \pm 0.012 \pm 0.002$	$31.5 \pm 1.0 \pm 3.7$	0.010	0.010
600	0	$0.0026 \pm 0.0006 \pm 0.0003$	$32.3 \pm 1.0 \pm 3.8$	0.0096	0.0099
700	0	$0.0008 \pm 0.0004 \pm 0.0001$	$33.3 \pm 1.1 \pm 3.4$	0.0091	0.0091
800	0	$0.0005 \pm 0.0003 \pm 0.00006$	$32.2 \pm 0.8 \pm 4.0$	0.0096	0.0096
900	0	$0.0002 \pm 0.0002 \pm 0.00002$	$33.2 \pm 0.8 \pm 3.8$	0.0094	0.0094
1000	0	$0.0002 \pm 0.0002 \pm 0.00003$	$33.3 \pm 0.9 \pm 3.9$	0.0093	0.0093

TABLE III: Selected data and expected SM background events for different excited electron masses. The efficiency for the signal is given as well. The first uncertainty is always statistical, the second systematic. Finally, the observed and the expected upper cross section limits for the production of single excited electrons with 95% CL are listed.

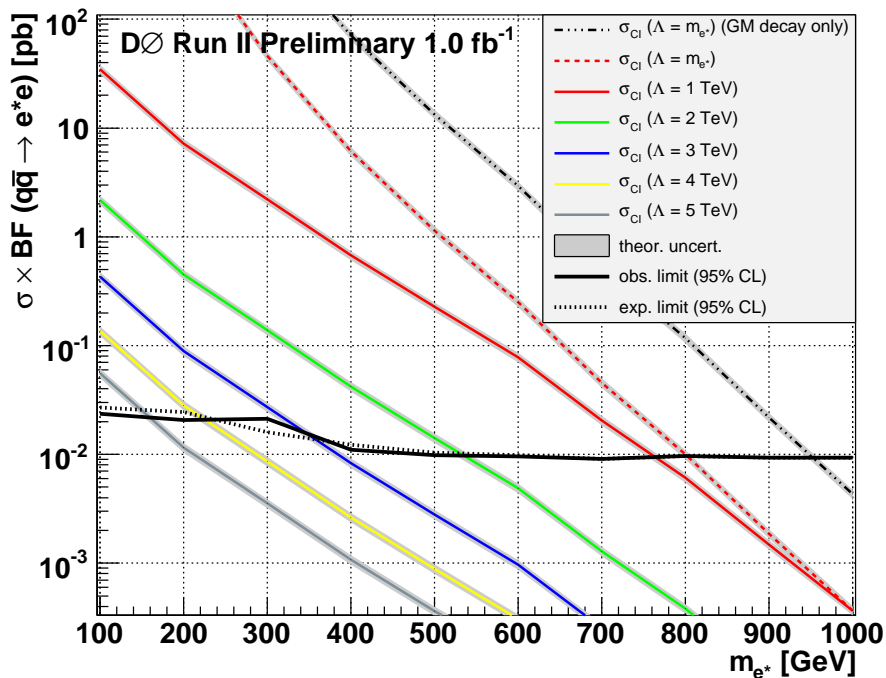


FIG. 6: Limits for the production cross section of single excited electrons at 95% CL. Also shown are different theoretical predictions, with the theoretical uncertainty indicated by grey shaded bands.

Acknowledgments

We thank the staffs at Fermilab and collaborating institutions, and acknowledge support from the DOE and NSF (USA); CEA and CNRS/IN2P3 (France); FASI, Rosatom and RFBR (Russia); CAPES, CNPq, FAPERJ, FAPESP and FUNDUNESP (Brazil); DAE and DST (India); Colciencias (Colombia); CONACyT (Mexico); KRF and KOSEF (Korea); CONICET and UBACyT (Argentina); FOM (The Netherlands); PPARC (United Kingdom); MSMT (Czech Republic); CRC Program, CFI, NSERC and WestGrid Project (Canada); BMBF and DFG (Germany); SFI (Ireland); The Swedish Research Council (Sweden); Research Corporation; Alexander von Humboldt Foundation; and the Marie

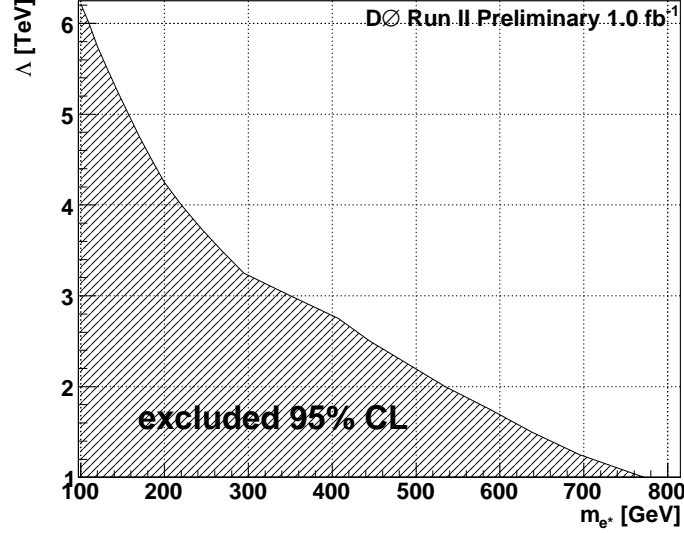


FIG. 7: The limit on the compositeness scale Λ at 95% CL as a function of the excited electron mass.

Curie Program.

-
- [1] H. Terazawa, M. Yasue, K. Akama and M. Hayashi, Phys. Lett. B **112**, 387 (1982); F.M. Renard, Il Nuovo Cimento **77** A, 1 (1983); A. De Rujula, L. Maiani and R. Petronzio, Phys. Lett. B **140**, 253 (1984); E.J. Eichten, K.D. Lane and M.E. Peskin, Phys. Rev. Lett. **50**, 811 (1983); M. A. Shupe, Phys. Lett. B **86**, 87 (1979).
 - [2] U. Baur, M. Spira and P.M. Zerwas, Phys. Rev. D **42**, 815 (1990).
 - [3] O. Cakir, C. Leroy, R. R. Mehdiyev and A. Belyaev, Eur. Phys. J. C **32S2**, 1 (2004).
 - [4] G. Abbiendi *et al.* (OPAL Collaboration), Phys. Lett. B **544**, 57 (2002); P. Achard *et al.* (L3 Collaboration), Phys. Lett. **B568**, 23 (2003); J. Abdallah *et al.* (DELPHI Collaboration), Eur. Phys. J. **C46**, 277 (2006); R. Barate *et al.* (ALEPH Collaboration), Eur. Phys. J. **C4**, 571 (1998).
 - [5] C. Adloff *et al.* (H1 Collaboration), Phys. Lett. **B548**, 35 (2002); S. Chekanov *et al.* (ZEUS Collaboration), Phys. Lett. **B549**, 32 (2002).
 - [6] D. Acosta *et al.* (CDF Collaboration), Phys. Rev. Lett. **94**, 101802 (2005).
 - [7] V.M. Abazov *et al.*, (D0 Collaboration), Nucl. Instrum. Methods Phys. Res. A **565**, 463 (2006).
 - [8] T. Andeen *et al.*, Fermilab-TM-2365-E, in preparation.
 - [9] T. Sjöstrand *et al.*, Comput. Phys. Commun. **135**, 238 (2001).
 - [10] R. Hamberg, W.L. van Neerven and T. Matsuura, Nucl. Phys. B **359**, 343 (1991).
 - [11] J.M. Campbell and R.K. Ellis, Phys. Rev. D **60**, 113006 (1999); J.M. Campbell and R.K. Ellis, <http://mcfm.fnal.gov/>.
 - [12] N. Kidonakis and R. Vogt, Int. J. Mod. Phys. A **20**, 3171 (2005).
 - [13] J. Pumplin *et al.*, JHEP **0207**, 012 (2002); D. Stump *et al.*, JHEP **0310**, 046 (2003).
 - [14] R. Brun and F. Carminati, CERN Program Library Long Writeup W5013, 1994 (unpublished).
 - [15] I. Bertram *et al.* (D0 Collaboration), FERMILAB-TM-2104 (2000).